Geometric phase estimation using time-frequency analysis

2001 J. Phys. A: Math. Gen. 34 8835

(http://iopscience.iop.org/0305-4470/34/42/308)

INSTITUTE OF PHYSICS PUBLISHING JOURNAL OF PHYSICS A: MATHEMATICAL AND GENERAL

J. Phys. A: Math. Gen. **34** (2001) 8835–8850 PII: S0305-4470(01)22424-X

Geometric phase estimation using time–frequency analysis

R Aleksiejunas[1] **and V Ivaska**

Department of Radiophysics, Vilnius University, Sauletekio al. 9 k. 3, LT-2040 Vilnius, Lithuania

E-mail: rimvydas.aleksiejunas@ff.vu.lt

Received 28 February 2001, in final form 21 August 2001
Published 12 October 2001
Online at stacks.iop.org/JPhysA/34/8835

Abstract

A method for geometric phase estimation from the scalar vector product of the initial- and final-state vectors of a system is proposed. The method is based on the time–frequency distribution, namely, the short-time Fourier transform (STFT) of a complex signal. By adjusting the width of the analysis window of the STFT, an estimated geometric phase can be obtained which closely matches a true geometric phase. The computational algorithm for geometric phase decomposition based on the Gabor expansion is presented. Numerical results are verified by several examples of geometric phase decompositions for $SU(2)$ evolutions.

PACS number: 03.65.Vf

1. Introduction

During the past decade, geometric phase theory has been extended from the original findings in quantum mechanics [1] to many areas of science including optics, solid state physics, chemistry and many others [2]. Having topological properties in common, geometric phases differ in the description techniques in all these cases. The most widely studied are the properties of geometric phase for $SU(2)$ polarization transformations [3]. Based on the analogy with polarized light waves, geometric phase decomposition has been proposed for scalar wave superpositions [4]. However, the method has limitations, because wave expansion into quasi-harmonic components must be performed prior to geometric phase decomposition, which restricts potential applications of the method. The components of the superposition are not exactly harmonic time series and cannot be determined from the resulting waveform unambiguously. The same difficulties arise in experimental observation of the geometric phase. In principle, all experiments reported to date have been based on some *a priori* information about a system's evolution. As a common case, system parameters are controlled in such a

[1] Corresponding author.

way that the dynamical phase is suppressed during cyclic evolution, and with the geometric phase left alone the total phase is measured. In other words, the geometric phase is not a directly observable quantity, but is deducible from the total phase. Moreover, there is no universal framework to obtain the geometric phase from the measured total phase without any knowledge of the theoretical model of the system.

Experimentally, the total phase of a system undergoing time evolution is measured as in-phase and quadrature components of some complex-valued signal, associated with the scalar vector product $\langle A|B\rangle$ of the initial- $|A\rangle$ and final- $|B\rangle$ state vectors. This is according to the Pancharatnam connection—the phase definition between two nonorthogonal vectors in Hilbert space [5,6]. Determination of the geometric phase from the resulting signal represents itself as a task of geometric phase decomposition of a complex signal. In this paper, we give a method for geometric phase decomposition for any complex signal with an arbitrary waveform, without the need for detailed information about the system's evolution. The method is restricted to systems governed by the dipole Hamiltonians, for which the evolution operator can be factorized by a combination of unitary operators, representing different types of dynamics. However, such systems constitute a large class of geometric phase manifestations, such as $SU(2)$-induced geometric phases of polarized waves [3] or spin-$\frac{1}{2}$ particles in a magnetic field [7, 8]. For the case of harmonic time series, the method generalizes the geometric phase decomposition for scalar wave superpositions [4]. The framework involves the time–frequency representation of complex signals, which represents the energy distribution simultaneously in the time and frequency domains. It allows us to differentiate between various kinds of dynamics and separate dynamical and geometric phases of the resulting waveform. The procedure is analogous to the geometric phase decomposition of the quantum state function in the noninteraction picture [9]. The only ambiguity that remains in such a decomposition is to choose which part of the evolution of the nonstationary system is due to free evolution and which to interaction. For a signal, an equivalent task is to determine the characteristic frequency, separating the frequency spectrum of free motion and interaction. We also present a computational algorithm for geometric phase decomposition, based on the Gabor expansion, which can be realized with the help of the fast Fourier transform. The numerical results of the method are verified by several examples of geometric phase decompositions for $SU(2)$ evolutions.

2. Geometric phase decomposition in the noninteraction picture

First let us briefly review the concept of geometric phase decomposition in the noninteraction picture [9], which later will serve as a starting point for geometric phase decomposition of a complex signal. If a free system is governed by a time-independent Hamiltonian H_0 and the corresponding evolution operator $U_0(t) = \exp\left(-\frac{\mathrm{i}}{\hbar}H_0 t\right)$, then the geometric phase for the initial $|\Psi_0(0)\rangle$ and final $|\Psi_0(t)\rangle$ states is expressed as

$$\gamma_0(t) = \arg\langle\Psi_0(0)|\ \Psi_0(t)\rangle + \frac{1}{\hbar}\int_0^t \langle\Psi_0(t')|H_0|\Psi_0(t')\rangle\,\mathrm{d}t' \tag{1a}$$

$$= \arg\langle\Psi_0(0)|U_0(t)|\Psi_0(0)\rangle + \frac{t}{\hbar}\,\langle\Psi_0(0)|\,H_0\,|\Psi_0(0)\rangle\,. \tag{1b}$$

The difference between the total and geometric phases, the dynamical phase, is a linear function of time in the case of a free system.

Consider now a system that is initially prepared in the eigenstate $|\Psi_0(0)\rangle = |m\rangle$ of H_0 and where interaction is turned on in such a way that the evolution operator becomes $U(t) = U_0(t)U_1(t)$, where $U_1(t)$ is the evolution operator due to interaction. This is the case

of nonadiabatic evolution governed by a dipole Hamiltonian (for more details see [9]). If the noninteraction picture is introduced in the way

$$|\Psi^{(0)}(t)\rangle = U_1^+(t)|\Psi(t)\rangle \qquad |\Psi^{(0)}(0)\rangle = |\Psi(0)\rangle = |m\rangle \tag{2}$$

$$H^{(0)}(t) = U_1^+(t)H(t)U_1(t) \tag{3}$$

with $|\Psi(t)\rangle$ and $H(t)$ being the state vector and the full Hamiltonian of the interacting system, respectively, then the geometric phase in the noninteraction picture is expressed in the usual form:

$$\gamma_m^{(0)}(t) = \arg\langle\Psi^{(0)}(0)|\Psi^{(0)}(t)\rangle + \frac{1}{\hbar}\int_0^t \langle\Psi^{(0)}(t')|H^{(0)}(t')|\Psi^{(0)}(t')\rangle\,\mathrm{d}t' \tag{4a}$$

$$= \arg\langle m(t)|\Psi(t)\rangle + \frac{1}{\hbar}\int_0^t \langle\Psi(t')|H(t')|\Psi(t')\rangle\,\mathrm{d}t' \tag{4b}$$

where the reference basis $\{|m(t)\rangle\}$ is time dependent and its time evolution is governed by the interaction evolution operator $U_1(t)$:

$$|m(t)\rangle = U_1(t)\,|m\rangle \qquad |m(0)\rangle = |m\rangle\,. \tag{5}$$

If the interaction Hamiltonian $H_1(t) = \mathrm{i}\hbar\dot{U}_1(t)U_1^+(t)$ has no diagonal matrix elements in the eigenbasis $\{|m\rangle\}$ of the free Hamiltonian, the geometric phase expression (4*b*) reduces to

$$\gamma_m^{(0)}(t) = \arg\langle m(t)|U_0(t)|m(t)\rangle + \frac{1}{\hbar}\int_0^t \langle m(t')|H_0|m(t')\rangle\,\mathrm{d}t' \tag{6}$$

which is similar to (1*a*), except that in the noninteraction picture the instantaneous eigenbasis $\{|m(t)\rangle\}$ is time dependent. This means that the geometric phase in the noninteraction picture possesses all the characteristics of the free geometric phase. Interaction only modifies the reference basis, which is equivalent to the change of initial state in (1*a*). Since in most cases $|H_1(t)| \ll |H_0|$, $U_1(t)$ represents slower evolution compared to $U_0(t)$. Therefore the behaviour of the geometric phase (6) may be regarded as if determined by free evolution $U_0(t)$ in the slowly varying instantaneous eigenbasis $\{|m(t)\rangle\}$.

3. Geometric phase decomposition for complex signals

There are many cases in history when quantum mechanical concepts have been successfully applied to signal analysis. These are the Wigner distribution, Cohen's class and the uncertainty principle in time–frequency analysis of complex signals [10, 11]. The main reason for this is that operator theory is widely used in both quantum physics and signal theory. Operators for time and frequency are established for continuous as well as for discrete time signals [10, 12].

Now we shall apply the concept of geometric phase decomposition in the noninteraction picture to complex signals. We shall require that the geometric phase defined for a complex signal satisfies the following criteria:

(i) it possesses the same characteristic features, nonlinearity and phase jumps, as the quantum geometric phase in the noninteraction picture;

(ii) it reduces to the geometric phase for scalar wave superpositions in the case of harmonic wave superposition.

Consider a complex signal

$$s(t) = A(t)\mathrm{e}^{\mathrm{i}\varphi(t)} \tag{7}$$

with $A(t)$ and $\varphi(t)$ being the amplitude and phase, respectively. Suppose that the energy of the signal is normalized to unity:

$$E = \int |s(t)|^2\,\mathrm{d}t = \int |A(t)|^2\,\mathrm{d}t = 1. \tag{8}$$

(All integrals without limits in this paper imply integration from $-\infty$ to $+\infty$.) In order to define the geometric phase in the noninteraction picture, we have to make an assumption about which part of the evolution may be considered as free evolution and which as interaction. If we consider a system which generates the signal to be free, the dynamical phase must be a linear function of time and correspond to a constant average frequency, which is defined as [10]

$$\langle\omega\rangle = \int s^*(t)\frac{1}{\mathrm{i}}\frac{\mathrm{d}}{\mathrm{d}t}s(t)\,\mathrm{d}t = \int S^*(\omega)\omega S(\omega)\,\mathrm{d}\omega \tag{9}$$

where $S(\omega)$ is the Fourier transform of a signal and '*' denotes the complex conjugate. When the signal's energy is properly normalized, $\frac{1}{\mathrm{i}}\frac{\mathrm{d}}{\mathrm{d}t}$ and ω have the meaning of frequency operators in the time and frequency domains, respectively, while $s(t)$ and $S(\omega)$ play the role of wavefunctions. The geometric phase is the difference between the total and dynamical phases:

$$\gamma_0(t) = \arg\left(s^*(0)s(t)\right) - \int_0^t \langle\omega\rangle\ \mathrm{d}t' = \arg\left(s^*(0)s(t)\right) - t\langle\omega\rangle. \tag{10}$$

This expression of geometric phase is analogous to the quantum geometric phase in the absence of interaction (1*b*). When a system is interacting, the dynamical phase is no longer a linear function of time, the time dependence of which is introduced through the time-dependent instantaneous eigenbasis $\{|m(t)\rangle\}$ (6). In a similar manner, to define the geometric phase for a complex signal, the reciprocal of the wavefunction $S(\omega)$ in the frequency domain must depend on time or, equivalently, $s(t)$ must be frequency dependent. This means that signal has to be characterized in both time and frequency simultaneously. Such a representation of a signal is known as a time–frequency distribution $P(t,\omega)$—the joint density of the signal's energy at time t and frequency ω. Ideally, the density $P(t,\omega)$ should satisfy the following marginal conditions:

$$P(t) = \int P(t,\omega)\,\mathrm{d}\omega = |s(t)|^2 \tag{11}$$

$$P(\omega) = \int P(t,\omega)\,\mathrm{d}t = |S(\omega)|^2 \tag{12}$$

$$\iint P(t,\omega)\,\mathrm{d}\omega\,\mathrm{d}t = \int |s(t)|^2\ \mathrm{d}t = \int |S(\omega)|^2\ \mathrm{d}\omega = 1. \tag{13}$$

Not all distributions satisfy the marginal conditions; therefore, in general, $P(t)$ and $P(\omega)$ should be used instead of $|s(t)|^2$ and $|S(\omega)|^2$, respectively. Substituting for $S^*(\omega)S(\omega) = |S(\omega)|^2$ the conditional time–frequency distribution $P(\omega|\,t) = P(t,\omega)/P(t)$ of frequency ω for a given time moment t, geometric phase expression (10) can be rewritten in a time-dependent 'eigenbasis' $P(t,\omega)$:

$$\gamma(t) = \arg\left(s^*(0)s(t)\right) - \int_0^t \langle\omega\rangle_{t'}\ \mathrm{d}t' = \arg\left(s^*(0)s(t)\right) - \int_0^t \frac{1}{P(t')}\int \omega P(t',\omega)\,\mathrm{d}\omega\,\mathrm{d}t' \tag{14}$$

where, instead of the average frequency $\langle\omega\rangle$, the instantaneous frequency $\langle\omega\rangle_t = \int \omega P(\omega|\,t)\,\mathrm{d}\omega$ is used. Integration over frequency ω in the dynamical phase part means averaging with a particular degree of smoothness depending on the form of the $P(t,\omega)$ distribution. By proper choice of $P(t,\omega)$, one may reach two ultimate cases of dynamical phase dependence on time: the first is a linear function with a constant frequency and the second dependence exactly follows the total phase. In terms of the noninteraction picture, this means two distinctive cases of free and interacting systems, and all the intermediate states have some part of the interaction transformed away by the noninteraction picture. One of the extreme cases, the free evolution, corresponds to factorization of the time–frequency distribution

$$P(t,\omega) = |s(t)|^2\,|S(\omega)|^2 \tag{15}$$

thus reducing the geometric phase expression (14) to (10). The second case, when the total evolution operator of a system is considered to be due to interaction, $U(t) = U_1(t)$, can be realized by the Wigner–Ville distribution [10, 11]:

$$P(t,\omega) = \frac{1}{2\pi}\int s^*(t-\tau/2)\, s(t+\tau/2)\, \mathrm{e}^{-\mathrm{i}\omega\tau}\,\mathrm{d}\tau$$
$$= \frac{1}{2\pi}\int S^*(\omega+\Omega/2)\, S(\omega-\Omega/2)\, \mathrm{e}^{-\mathrm{i}\Omega t}\,\mathrm{d}\Omega. \tag{16}$$

For such a distribution, the dynamical phase part approaches the total phase and the geometric phase vanishes:

$$\gamma(t) = \varphi(t) - \int_0^t \varphi'(t')\,\mathrm{d}t' = 0 \tag{17}$$

because the mean instantaneous frequency of the Wigner–Ville distribution is equal to the mean instantaneous frequency of the complex signal, $\langle\omega\rangle_t = \varphi'(t)$ [10, 11]. To cover all intermediate cases, one needs a distribution $P(t,\omega)$ which has a parameter to adjust the form of the distribution in order to produce the mean frequency of the dynamical phase between a constant $\omega_0 = \langle\omega\rangle$ and total phase derivative $\varphi'(t)$. A good candidate for such a distribution may be the short-time Fourier transform (STFT) [10, 11]:

$$P(t,\omega) = |\mathrm{STFT}(t,\omega)| \tag{18}$$

$$\mathrm{STFT}(t,\omega) = \frac{1}{\sqrt{2\pi}}\int s(\tau)g^*(\tau-t)\,\mathrm{e}^{-\mathrm{i}\omega\tau}\,\mathrm{d}\tau \tag{19}$$

where $g(t)$ is a window function, called the analysis window. It balances the time and frequency resolutions. If a function has a short time duration, its frequency bandwidth is wide, and vice versa. This is analogous to the quantum mechanical uncertainty principle—the better the frequency resolution achieved, the poorer the time resolution will be, and vice versa. The optimal concentration of the signal's energy in the joint time–frequency domain is achieved when a real Gaussian function is used

$$g(t) = \left(\frac{\sigma^2}{\pi}\right)^{\frac{1}{4}} \exp\left(-\frac{\sigma^2 t^2}{2}\right) \tag{20}$$

where σ defines the width of the window and the amplitude factor is chosen for energy normalization to unity. The time duration Δ_t and frequency bandwidth Δ_ω of the Gaussian function are defined by the standard deviations [10]:

$$\Delta_t^2 = \int (t-\langle t\rangle)^2\,|g(t)|^2\,\mathrm{d}t = \frac{1}{2\sigma^2} \tag{21}$$

$$\Delta_\omega^2 = \int (\omega-\langle\omega\rangle)^2\,|G(\omega)|^2\,\mathrm{d}\omega = \frac{\sigma^2}{2} \tag{22}$$

where $G(\omega) = \left(\sigma^2\pi\right)^{1/4}\exp\left(-\omega^2/2\sigma^2\right)$ is the Fourier transform of $g(t)$; mean time $\langle t\rangle$ and mean frequency $\langle\omega\rangle$ are equal to zero. (In some of the literature, the time duration and frequency bandwidth are defined as $2\Delta_t$ and $2\Delta_\omega$, respectively [11].) For the Gaussian window, the uncertainty principle $\Delta_t\Delta_\omega \geqslant 1/2$ becomes the equality $\Delta_t\Delta_\omega = 1/2$, which indicates the best resolution in the time–frequency plane.

Smaller σ values correspond to better resolution in the frequency domain, and greater values to better resolution in the time domain. Consequently, the σ parameter can be used to control the smoothness of the dynamical phase time dependence, acquired by integrating the mean frequency of the STFT distribution. In other words, σ can be prescribed the meaning of an intermediate frequency between free evolution and interaction. As a common case, free

evolution differs from interaction by the greater field values, thus resulting in higher-frequency oscillations, described by corresponding dipole Hamiltonians. Interaction only modifies free evolution by introducing relatively lower frequencies. (An example may be a spin in a strong magnetic field interacting with the rotating magnetic field of a plane wave. Here free evolution means spin precession about a constant field axis, while the interaction produces nutation of the precession axis with frequency much less than the precession frequency.)

Therefore, frequencies that are higher than σ are averaged out and the time–frequency distribution $P(t,\omega)$ contains only lower frequencies of interaction. When evaluating dynamical phase as an integral of the mean frequency of the $P(t,\omega)$ distribution, it looks as if 'eigenbasis' $P(t,\omega)$ is governed by the interaction, a part of the total evolution of the interacting system. This is just the same concept as follows from the geometric phase decomposition in the noninteraction picture for the quantum case.

Generally, for real-world signals the meaning of free evolution and interaction of an original system is not known *a priori* and σ becomes an independent variable. Since the frequencies lying to the right of σ are smeared out in the time–frequency distribution, by varying σ one may observe resulting effects on the dynamical phase evolution induced by the rest of the lower frequencies. In this way, σ is closely related to the dynamics, which generates the signal.

Now we shall prove that two limit values of σ, i.e. zero and infinity, correspond to the two extreme cases of dynamical phase instantaneous frequency $\langle\omega\rangle_t$, namely, a constant ω_0 and total phase derivative $\varphi'(t)$.

When $\sigma \to 0$, $\mathrm{STFT}(t,\omega)$ becomes time independent, which results in a constant instantaneous frequency:

$$\langle\omega\rangle_t = \frac{\int \omega \left|\mathrm{STFT}(t',\omega)\right| \mathrm{d}\omega}{\int |\mathrm{STFT}(t',\omega)| \mathrm{d}\omega} = \mathrm{const} \equiv \omega_0. \tag{23}$$

To study the case $\sigma \to \infty$, let us define a new signal $\tilde{s}(t) = \tilde{A}(t)\mathrm{e}^{\mathrm{i}\tilde{\varphi}(t)}$ with the Fourier transform

$$\widetilde{\mathrm{STFT}}(t,\omega) = |\mathrm{STFT}(t,\omega)|^{1/2}\, \mathrm{e}^{\mathrm{i}\arg(\mathrm{STFT}(t,\omega))}. \tag{24}$$

For the case $\sigma \to \infty$, it follows from the Dirac function representation $\delta(t) = \frac{\sigma}{\sqrt{\pi}}\mathrm{e}^{-\sigma^2 t^2}$, $\sigma \to \infty$ that the window function approaches the delta function, $g(t) \to \sqrt{\delta(t)}$, and in the limit

$$\begin{aligned} |\mathrm{STFT}(t,\omega)|^2 &= \mathrm{STFT}^*(t,\omega)\mathrm{STFT}(t,\omega) \\ &= \frac{1}{2\pi}\iint s^*(\tau_1)s(\tau_2)\sqrt{\delta(\tau_1-t)\delta(\tau_2-t)}\mathrm{e}^{-\mathrm{i}\omega(\tau_2-\tau_1)}\,\mathrm{d}\tau_1\,\mathrm{d}\tau_2 \\ &= \frac{1}{2\pi}\int |s(\tau)|^2\,\delta(\tau-t)\,\mathrm{d}\tau = \frac{1}{2\pi}\,|s(t)|^2 = \frac{1}{2\pi}A(t)^2 \end{aligned} \tag{25}$$

and, equivalently,

$$\left|\widetilde{\mathrm{STFT}}(t,\omega)\right|^2 = \frac{1}{2\pi}\tilde{A}(t)^2. \tag{26}$$

From (24)–(26) it follows that in the limit $\sigma \to \infty$

$$\left|\widetilde{\mathrm{STFT}}(t,\omega)\right| = |\mathrm{STFT}(t,\omega)|^{1/2} = (2\pi)^{-1/4}\,A^{1/2}(t) = (2\pi)^{-1/2}\,\tilde{A}(t) \tag{27}$$

which means that it is possible to construct $\tilde{s}(t)$ with the same phase as $s(t)$, $\tilde{\varphi}(t) = \varphi(t)$, and amplitude $\tilde{A}(t) = (2\pi)^{1/4}\,A^{1/2}(t)$ satisfying relation (24) for $\sigma \to \infty$. Since in the limit $\sigma \to \infty$, $\left|\widetilde{\mathrm{STFT}}(t,\omega)\right|$ as well as $|\mathrm{STFT}(t,\omega)|$ do not depend on ω, averaging over frequency

in the instantaneous frequency expression must be replaced by integration over the time axis, in analogy to (9). Hence, the instantaneous frequency can be calculated in terms of the new signal as

$$\begin{aligned}\langle\omega\rangle_t &= \frac{\int \omega\,|\mathrm{STFT}(t,\omega)|\,\mathrm{d}\omega}{\int |\mathrm{STFT}(t,\omega)|\,\mathrm{d}\omega} = \frac{1}{\tilde{P}(t)}\int \widetilde{\mathrm{STFT}}^{*}(t,\omega)\omega\widetilde{\mathrm{STFT}}(t,\omega)\,\mathrm{d}\omega \\ &= \int \tilde{\eta}_t^{*}(\tau)\frac{1}{\mathrm{i}}\frac{\mathrm{d}}{\mathrm{d}t}\tilde{\eta}_t(\tau)\,\mathrm{d}\tau = \frac{1}{\tilde{P}(t)}\int \tilde{A}^2(\tau)\frac{\sigma}{\sqrt{\pi}}\mathrm{e}^{-\sigma^2(\tau-t)^2}\varphi'(\tau)\,\mathrm{d}\tau \\ &= \frac{\int \tilde{A}^2(\tau)\frac{\sigma}{\sqrt{\pi}}\mathrm{e}^{-\sigma^2(\tau-t)^2}\varphi'(\tau)\,\mathrm{d}\tau}{\int \tilde{A}^2(\tau)\frac{\sigma}{\sqrt{\pi}}\mathrm{e}^{-\sigma^2(\tau-t)^2}\,\mathrm{d}\tau} \underset{\sigma\to\infty}{\to} \frac{\int \tilde{A}^2(\tau)\delta(\tau-t)\varphi'(\tau)\,\mathrm{d}\tau}{\int \tilde{A}^2(\tau)\delta(\tau-t)\,\mathrm{d}\tau} = \varphi'(t) \end{aligned} \tag{28}$$

where $\tilde{P}(t)$ is the time marginal of $\widetilde{\mathrm{STFT}}(t,\omega)$:

$$\tilde{P}(t) = \int \left|\widetilde{\mathrm{STFT}}(t,\omega)\right|^2 \mathrm{d}\omega = \int |\tilde{s}(\tau)|^2\,|g(\tau-t)|^2\,\mathrm{d}\tau = \int \tilde{A}^2(\tau)\frac{\sigma}{\sqrt{\pi}}\mathrm{e}^{-\sigma^2(\tau-t)^2}\,\mathrm{d}\tau \tag{29}$$

and $\tilde{\eta}_t(\tau) = \tilde{P}(t)^{-1/2}\tilde{s}(\tau)g(\tau-t)$ is a signal, normalized in the variable τ, $\int |\tilde{\eta}_t(\tau)|^2\,\mathrm{d}\tau = 1$ [10]. Therefore, as expected, the STFT can cover the full range of dynamical phase behaviour by adjusting the window width σ.

Next we shall show that geometric phase decomposition of a complex signal reduces to the geometric phase decomposition for scalar waves [4], if it is applied to a harmonic time series

$$s(t) = \sum_n a_n \mathrm{e}^{\mathrm{i}\omega_n t} \tag{30}$$

where a_n are real positive amplitudes and ω_n are angular frequencies, respectively. In order to obtain a linear time dependence of the dynamical phase, the window length must approach zero: $\sigma \to 0$. As pointed out in [4], for scalar wave superpositions, averaging over frequency in the dynamical phase expression must be performed with respect to the amplitudes of the waves, not intensities. Note that, for this reason, the amplitude of the STFT is chosen as a time–frequency distribution in (18) instead of the usual power density. Inserting signal expansion (30) into the expression of instantaneous frequency (23), and integrating the dynamical phase part of (14), yields

$$\begin{aligned}\alpha(t) &= \int_0^t \frac{1}{P(t')}\int \omega P(t',\omega)\,\mathrm{d}\omega\,\mathrm{d}t' = \int_0^t \frac{\int \omega\left|\mathrm{STFT}(t',\omega)\right|\mathrm{d}\omega}{\int \left|\mathrm{STFT}(t',\omega)\right|\mathrm{d}\omega}\,\mathrm{d}t' \\ &= \int_0^t \frac{\int \omega\left|\frac{1}{\sqrt{2\pi}}\int \sum_n a_n \mathrm{e}^{\mathrm{i}(\omega_n-\omega)\tau}\left(\frac{\sigma^2}{\pi}\right)^{\frac{1}{4}}\mathrm{e}^{-\frac{\sigma^2}{2}(\tau-t')^2}\,\mathrm{d}\tau\right|\mathrm{d}\omega}{\int \left|\frac{1}{\sqrt{2\pi}}\int \sum_n a_n \mathrm{e}^{\mathrm{i}(\omega_n-\omega)\tau}\left(\frac{\sigma^2}{\pi}\right)^{\frac{1}{4}}\mathrm{e}^{-\frac{\sigma^2}{2}(\tau-t')^2}\,\mathrm{d}\tau\right|\mathrm{d}\omega}\,\mathrm{d}t' \\ &\underset{\sigma\to 0}{\to} \int_0^t \frac{\int \omega\left|\sum_n a_n\delta(\omega_n-\omega)\right|\mathrm{d}\omega}{\int \left|\sum_n a_n\delta(\omega_n-\omega)\right|\mathrm{d}\omega}\,\mathrm{d}t' = \frac{\sum_n a_n\omega_n t}{\sum_n a_n}. \end{aligned} \tag{31}$$

The geometric phase, as a difference between the total and dynamical phases, is

$$\gamma(t) = \arg(s^{*}(0)s(t)) - \alpha(t) = \arctan\left(\frac{\sum_n a_n \sin\omega_n t}{\sum_n a_n\cos\omega_n t}\right) - \frac{\sum_n a_n\omega_n t}{\sum_n a_n} \tag{32}$$

which is in accordance with the proposed decomposition in [4].

Hence, we have shown that the geometric phase for a complex signal is a generalization of the geometric phase decompositions in the noninteraction picture and for scalar wave superpositions.

4. Computation of time–frequency distribution

The STFT, which we have used to obtain the time–frequency distribution for dynamical phase averaging, has a dual transform—the inverse STFT [10, 11]:

$$s(t) = \frac{1}{\sqrt{2\pi}\, g^*(0)} \int \mathrm{STFT}(t, \omega) \mathrm{e}^{\mathrm{i}\omega t}\, \mathrm{d}\omega. \tag{33}$$

This comes in a pair for STFT for continuous time and frequency signals but cannot be used in numerical analysis of sampled signals. Moreover, the inverse STFT (33) is a highly redundant representation of a signal [11]. Indeed, even a continuous-time signal can be reconstructed merely from the sampled version of the STFT [11]:

$$\mathrm{STFT}\,[mT, k\Omega] = \int s(t) g^*(t - mT) \mathrm{e}^{-\mathrm{i}k\Omega t}\, \mathrm{d}t = \int s(t) g^*_{mk}(t)\, \mathrm{d}t \tag{34}$$

$$s(t) = \sum_{m=-\infty}^{\infty} \sum_{k=-\infty}^{\infty} \mathrm{STFT}\,[mT, k\Omega]\, h(t - mT) \mathrm{e}^{\mathrm{i}k\Omega t} = \sum_{m=-\infty}^{\infty} \sum_{k=-\infty}^{\infty} \mathrm{STFT}\,[mT, k\Omega]\, h_{mk}(t) \tag{35}$$

where T and Ω denote the time and frequency sampling steps, respectively, and $g_{mk}(t)$ and $h_{mk}(t)$ are time-shifted and frequency-modulated dual functions

$$g_{mk}(t) = g(t - mT) \mathrm{e}^{\mathrm{i}k\Omega t} \tag{36}$$

$$h_{mk}(t) = h(t - mT) \mathrm{e}^{\mathrm{i}k\Omega t} \tag{37}$$

which have to satisfy two bi-orthonormality conditions:

$$\sum_{m=-\infty}^{\infty} \sum_{k=-\infty}^{\infty} g^*_{mk}(t) h_{mk}(t') = \delta(t - t') \tag{38}$$

$$\int g^*_{mk}(t) h_{nl}(t)\, \mathrm{d}t = \delta\,[m - n]\, \delta\,[k - l] \tag{39}$$

where $\delta(t)$ and $\delta\,[m]$ are the continuous and discrete Dirac functions and square brackets throughout denote functions of discrete variables.

Sampled versions of the STFT and inverse STFT are known as the Gabor transform and Gabor expansion, respectively, after Dennis Gabor, who first invented two-dimensional signal representation by elementary functions localized both in time and frequency [13]:

$$s(t) = \sum_{m=-\infty}^{\infty} \sum_{k=-\infty}^{\infty} A_{mk} h_{mk}(t) \tag{40}$$

where $A_{mk} = \mathrm{STFT}\,[mT, k\Omega]$ are called Gabor coefficients. The necessary condition for existence of the Gabor expansion is that the sampling steps T and Ω must be small enough to satisfy

$$T\Omega \leqslant 2\pi. \tag{41}$$

The case when $T\Omega = 2\pi$ is called critical sampling and that when $T\Omega < 2\pi$ oversampling. Only for the critical sampling are Gabor elementary functions $\{h_{mk}(t)\}$ linearly independent and dual functions $\{g_{mk}(t)\}$ unique and bi-orthogonal to $\{h_{mk}(t)\}$. In order that Gabor coefficients could represent the signal's behaviour in the joint time–frequency domain, dual functions $\{g_{mk}(t)\}$, which play the role of windowing functions in (34), must be concentrated in both the time and frequency domains. The optimal choice is the one whose shape is closest to $\{h_{mk}(t)\}$, the Gaussian functions, in the sense of the least-squares error,

$$\Delta_{mk} = \min_{-\infty < t < \infty} |g_{mk}(t) - h_{mk}(t)|^2\,. \tag{42}$$

As the oversampling rate increases, the error Δ_{mk} becomes smaller, and in the limit $g_{mk}(t) = \text{const} \cdot h_{mk}(t)$, for which case (34), (35) are called the orthogonal-like Gabor transform.

To obtain the discrete version of the Gabor transform, suitable for analysis of discrete signals, both time and frequency axes need to be sampled. Remember that sampling of one domain leads to periodicity in the adjacent domain. After sampling a signal $s(t)$ in the time and frequency domains by substitutions

$$t \to n \qquad T \to N \qquad \Omega \to 2\pi/K \tag{43}$$

with n being a discrete variable and N and K being integer numbers, Gabor coefficients A_{mk} become periodic in both m and k variables with integer periods M and K, respectively, where M satisfies the condition [14]

$$MN \geqslant N_{\mathrm{s}} + N_{\mathrm{g}} - 1 \tag{44}$$

with N_{s} and N_{g} being the finite supports of a signal and window function, respectively. After this we obtain a pair of discrete Gabor expansion-transforms [14]:

$$s[n] = \sum_{m=\langle M\rangle} \sum_{k=\langle K\rangle} A_{mk} h[n - mN] \, \mathrm{e}^{\mathrm{i}2\pi nk/K} \tag{45}$$

$$A_{mk} = \sum_{n=\langle MN\rangle} s[n] \, g^*[n - mN] \, \mathrm{e}^{-\mathrm{i}2\pi nk/K} \tag{46}$$

where the expression $m = \langle M\rangle$ throughout denotes a finite interval of M successive integers m. Now the condition (41) for sampling steps becomes

$$N/K \leqslant 1 \tag{47}$$

and the degree of oversampling is expressed as $K/N = p/q \geqslant 1$, where p and q are two integers ($p \geqslant q \geqslant 1$) that do not have common factors.

The discrete Gabor transform can be calculated using computer algorithms based on the fast Fourier transform. One such algorithm, which we have used in numerical analysis, is presented in [14]. In order to determine Gabor coefficients, it uses discrete Fourier and discrete Zak transforms, for which fast Fourier transforms can be applied.

5. Numerical results

The proposed method is verified by a number of geometric phase decompositions reported earlier in the literature [9,15–20]. These cases represent exact decompositions using theoretical models of $SU(2)$ evolutions except for [15], based on experimental observations.

Many other experimental results of geometric phase observations cannot be analysed by the STFT method because they are available only for closed paths in the parametric space. Experimentally, the geometric phase is obtained from the total phase in polarimetric [18] or interferometric [21] measurements, when system parameters are controlled in such a way as to suppress the dynamical phase part. Although various experiments have been conducted, including cyclic [8] as well as noncyclic [15] state evolutions, most of them are aimed at measuring the phase shift after the system undergoes some finite-length evolution in time or space. This means that the measured quantity represents a complete geometric phase but not the phase evolution itself, the intermediate points, required to justify numerical results of the method. There are experiments on geometric phase reporting quantum beats of intensity versus time [22–24]. However, these are also concerned with a static (or quasi-static [24]) phase shift introduced by particular evolution, and the beats of intensity are useful only for determination of the phase shift.

Numerical simulations are applied to a complex signal $s(t)$ reconstructed from the scalar vector product of the state vector $|\Psi(t)\rangle$ and initial state $|m(t)\rangle$, which, in general, can be time dependent:

$$s(t) = \langle m(t)|\ \Psi(t)\rangle = |\langle m(t)|\ \Psi(t)\rangle|\, \mathrm{e}^{\mathrm{i}\beta(t)} \tag{48}$$

where $\beta(t)$ is the total phase. The geometric phase of the complex signal estimated by the time–frequency analysis is compared with that calculated theoretically in the corresponding original papers. The particular values of the system parameters in the following examples are chosen according to the original works.

5.1. Spin $\frac{1}{2}$ in a static magnetic field

Interferometric amplitudes and phases of the polarized neutrons in a constant magnetic field have been measured and verified by theoretical results in [15]. Spin-$\frac{1}{2}$ particles with spins initially subtending an angle θ with a static magnetic field undergo a precession with an angle ϕ_{L} as determined by the $SU(2)$ transformation $\exp(-\mathrm{i}\sigma_z\phi_{\mathrm{L}}/2)$, where σ_z is the third Pauli matrix. Interference between initial and final states results in a complex signal $s(\phi_{\mathrm{L}}) = A(\phi_{\mathrm{L}})\mathrm{e}^{\mathrm{i}\beta(\phi_{\mathrm{L}})}$ with amplitude and phase [15]

$$A(\phi_{\mathrm{L}}) = \sqrt{1 - \sin^2\theta\ \sin^2\frac{\phi_{\mathrm{L}}}{2}} \tag{49}$$

$$\beta(\phi_{\mathrm{L}}) = -\arctan\left(\cos\theta\ \tan\frac{\phi_{\mathrm{L}}}{2}\right). \tag{50}$$

The corresponding geometric phase for noncyclic evolutions is given by

$$\gamma(\phi_{\mathrm{L}}) = -\arctan\left(\cos\theta\ \tan\frac{\phi_{\mathrm{L}}}{2}\right) + \frac{\phi_{\mathrm{L}}}{2}\cos\theta. \tag{51}$$

Numerically the geometric phase is estimated by applying the STFT with oversampling $K/N = 128$ to the 512-point sampled complex signal. The width of the Gaussian window (20) is chosen as $\sigma = 0.75 \cdot 2\pi/T$ with respect to the period of precession $T = 360^\circ$. For such a window width, the dynamical phase linearly depends on ϕ_{L} and the estimated geometric phase closely matches the theoretical dependence as shown in figure 1. However, in order to achieve the desired resemblance, not only does the window width have to be adjusted, but also the minimum STFT spectrum level must be set. This is because even the small variations of the spectrum due to sampling effects produce significant errors in averaging over frequency in the dynamical phase expression (14). In this case, only spectral components greater than 10^{-3} of the maximum value are taken into account.

5.2. Spin $\frac{1}{2}$ in a rotating magnetic field

For a spin-$\frac{1}{2}$ particle subjected to an external magnetic field $\boldsymbol{B}(t) = (B_1\cos\omega t, B_1\sin\omega t, B_0)$ rotating with Larmor frequency $\omega = \omega_0 = g'B_0$ (g' is the gyromagnetic ratio) the scalar vector product for the initial state $m = 1/2$ is expressed as [9]

$$s(t) = \langle m(t)|\ \Psi(t)\rangle = \left\langle \frac{1}{2}\right| U_{\mathrm{I}}^{+}(t)U(t)\left|\frac{1}{2}\right\rangle = \cos\frac{\omega_0 t}{2} - \mathrm{i}\cos\omega_1 t\ \sin\frac{\omega_0 t}{2} \tag{52}$$

which represents a complex signal by itself (here $\omega_1 = g'B_1$). In figure 2, the numerically obtained geometric phase is compared with the theoretical dependence [9]

$$\gamma(t) = -\arctan\left[\cos\omega_1 t\ \tan\frac{\omega_0 t}{2}\right] + \frac{\omega_0}{2}\frac{\sin\omega_1 t}{\omega_1} \tag{53}$$

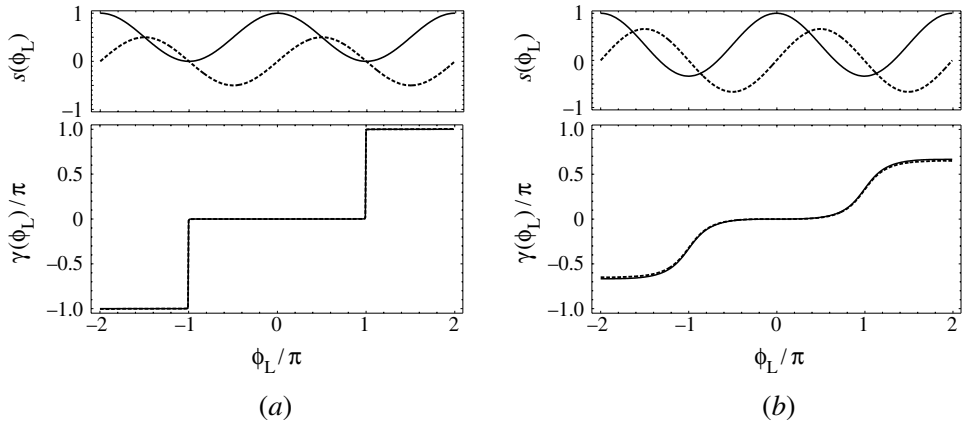

Figure 1. Geometric phase decomposition for a spin $\frac{1}{2}$ in a static magnetic field for different angles of incident spin orientation θ: 90.01° (*a*) and 109.5° (*b*). Top of each plot, real (solid curve) and imaginary (dashed curve) parts of the complex signal. Bottom of each plot, true (solid curve) and estimated (dashed curve) geometric phases. STFT parameters: window width $\sigma = 0.75 \cdot 2\pi/T$, $T = 360^\circ$, oversampling $K/N = 128$ and minimum spectral level 10^{-3}.

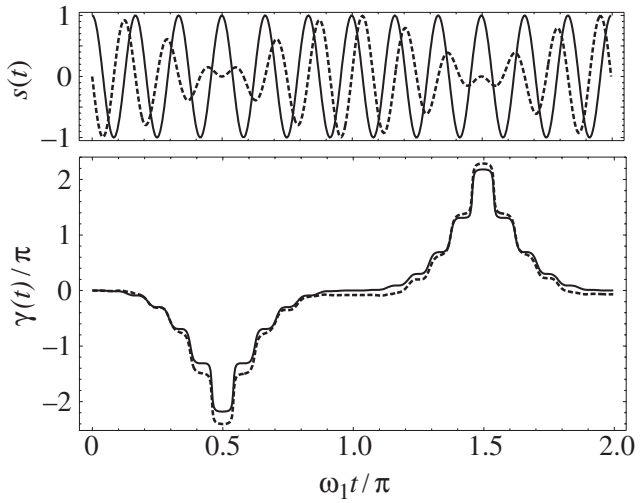

Figure 2. Geometric phase decomposition for a spin $\frac{1}{2}$ in a rotating magnetic field for a cyclic state with period $T = 2\pi/\omega_1$ and $\omega_0 T = 48\pi$. Top, real (solid curve) and imaginary (dashed curve) parts of the complex signal. Bottom, true (solid curve) and estimated (dashed curve) geometric phases. STFT parameters: window width $\sigma = 1.324\omega_1 = 0.055\omega_0$, oversampling $K/N = 128$ and minimum spectral level 0.2.

for a cyclic state with period $T = 2\pi/\omega_1$ and $\omega_0 T = 48\pi$. The complex signal is sampled by 512 points and then STFT with oversampling $K/N = 128$ and minimum spectrum level 0.2 is applied. The parameter σ of the window, or frequency bandwidth, is set to $\sigma = 1.324\omega_1 = 0.055\omega_0$, i.e. $\omega_1 < \sigma < \omega_0$. This means that STFT with such a window filters out the high-frequency ω_0 component and leaves only ω_1 oscillations in the dynamical phase. As is evident from figure 2, there is quite good agreement between the true and estimated geometric phases.

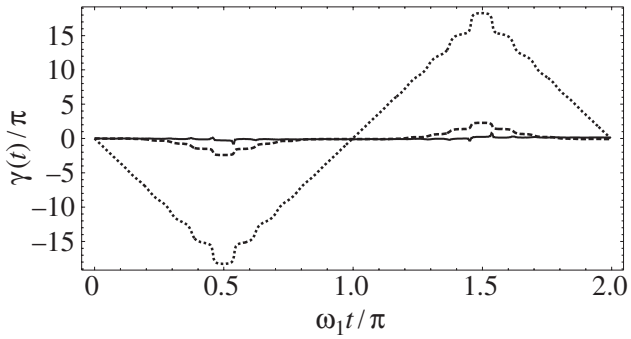

Figure 3. Estimated geometric phase of a spin $\frac{1}{2}$ in a rotating magnetic field for the same evolution as in figure 2, but different widths of STFT window: $\sigma = 225\omega_1 = 9.375\omega_0$ (solid curve), $\sigma = 1.324\omega_1 = 0.055\omega_0$ (dashed curve) and $\sigma = 0.225\omega_1 = 0.9375 \times 10^{-3}\omega_0$ (dotted curve).

Varying the STFT window width, two extreme cases of geometric phase dependence can be achieved. Narrowing the window, when $\sigma = 225\omega_1 = 9.375\omega_0$ and $\omega_1 < \omega_0 < \sigma$, the dynamical phase approaches the total phase and the geometric phase vanishes. For a wide window with $\sigma = 0.225\omega_1 = 0.9375 \times 10^{-3}\omega_0$ when $\sigma < \omega_1 < \omega_0$, the dynamical phase becomes constant and equal to zero. In this case, the geometric phase coincides with the total phase. This situation is illustrated in figure 3 and represents different choices between free evolution and interaction of a corresponding system as discussed in section 2.

A rotating magnetic field with $B_1 \ll B_0$ is usually encountered in magnetic resonance experiments such as [7]. Yet another configuration of rotating magnetic field is used in neutron polarimetry [18]. Consider polarized-spin neutrons [16–18] subjected to a magnetic field of constant amplitude B_1 rotating with the angular frequency ω in the xy plane: $\boldsymbol{B}(t) = (B_1 \cos\omega t, B_1 \sin\omega t, 0)$. For neutrons with spin oriented along the stationary effective field $\boldsymbol{B}_\mathrm{r} = (B_1, 0, -\omega/g')$ [16, 17], subtending an angle θ with the z axis, the scalar vector product of the initial $|\Psi(0)\rangle$ and final $|\Psi(t)\rangle$ states is

$$s(t) = \langle\Psi(0)|\ \Psi(t)\rangle = \mathrm{e}^{-\mathrm{i}\frac{\omega_\mathrm{r} t}{2}} \left(\cos\frac{\omega t}{2} - \mathrm{i}\cos\theta\ \sin\frac{\omega t}{2}\right) \tag{54}$$

where $\omega_\mathrm{r} = g'|\boldsymbol{B}_\mathrm{r}|$, and the geometric phase at time t becomes [16, 18]

$$\gamma(t) = -\arctan\left[\cos\theta\ \tan\frac{\omega t}{2}\right] + \frac{\omega t}{2}\cos\theta. \tag{55}$$

The estimated geometric phase for effective field angle $\theta = 105^\circ$ is obtained from a 512-point sampled signal and compared with the true dependence in figure 4. For a chosen set of STFT parameter values, the approximation closely follows the true geometric phase.

5.3. Polarization rotation

Consider a plane wave subjected to polarization rotation in an optically active medium, or Faraday effect. For a linearly polarized wave consisting of two circularly polarized components $\boldsymbol{e}_+$, $\boldsymbol{e}_-$, with ellipticity parameter $Z = |\boldsymbol{e}_+|^2 - |\boldsymbol{e}_-|^2$, the scalar vector product of the initial $\boldsymbol{e}(0)$ and final $\boldsymbol{e}(z)$ polarization vectors is expressed as [19]

$$s(z) = \boldsymbol{e}^*(0)\boldsymbol{e}(z) = \mathrm{e}^{\mathrm{i}\kappa z}\,(\cos\delta z + \mathrm{i}Z\sin\delta z) \tag{56}$$

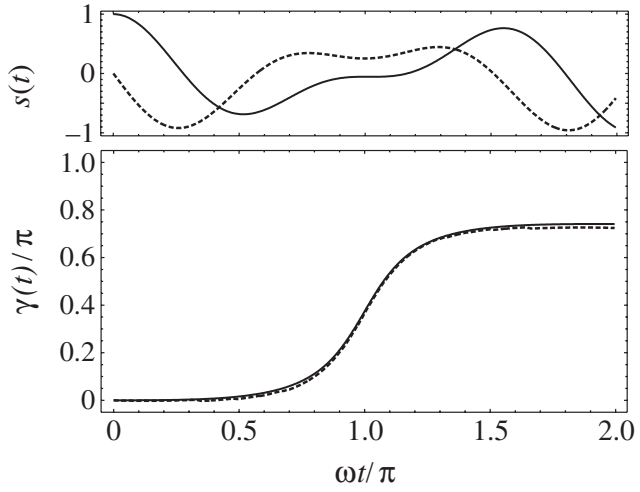

Figure 4. Geometric phase decomposition for a spin $\frac{1}{2}$ in a rotating magnetic field with spin oriented along the effective field making an angle $\theta = 105^\circ$ with the z axis. Top, real (solid curve) and imaginary (dashed curve) parts of the complex signal. Bottom, true (solid curve) and estimated (dashed curve) geometric phases. STFT parameters: window width $\sigma = 0.90 \cdot 2\pi/T$, $T = 360^\circ$, oversampling $K/N = 128$ and minimum spectral level 0.05.

where $\kappa = (k_+ + k_-)/2$ is the average wavenumber and $\delta = (k_+ - k_-)/2$ is the difference between the wavenumbers $k_\pm$ of two circularly polarized components propagating along the z direction. The geometric phase evaluated analytically [19]

$$\gamma(z) = \arctan(Z \tan \delta z) - Z\delta z \tag{57}$$

together with the complex signal (56) are shown in figure 5 for parameter values $Z = 0.05$ and $\delta = 0.2\kappa$. Here is also shown the geometric phase estimated from the 256-point sampled complex signal. For a chosen STFT window bandwidth $\sigma = 0.75\delta = 0.15\kappa$ when $\sigma < \delta < \kappa$, oversampling $K/N = 64$ and minimum spectral level 10^{-2}, the dynamical phase is averaged down to linear dependence and the resulting geometric phase shows good agreement with theoretical results.

5.4. Birefringence

Another type of polarization transformation is birefringence—change of polarization ellipticity when a plane wave propagates through materials in which the index of refraction depends on the alignment of the linear polarization. When a plane wave linearly polarized along the x axis passes through a birefringent plate with retardation δ, its fast axis making an angle β with the x axis, the scalar product of the polarization vectors can be written as [20]

$$s(\beta) = \boldsymbol{e}^*(0)\boldsymbol{e}(\beta) = a(\beta)\mathrm{e}^{\mathrm{i}\phi(\beta)} \tag{58}$$

where amplitude $a(\beta)$ and phase $\phi(\beta)$ are determined by the following equations:

$$a(\beta)\cos[\phi(\beta)] = \cos^2\beta + \sin^2\beta\cos\delta \tag{59}$$

$$a(\beta)\sin[\phi(\beta)] = \sin^2\beta\sin\delta. \tag{60}$$

The geometric phase is expressed as the difference between the total $\phi(\beta)$ and dynamical $\phi_\mathrm{d}(\beta)$ phases [20]:

$$\gamma(\beta) = \phi(\beta) - \phi_\mathrm{d}(\beta) \tag{61}$$

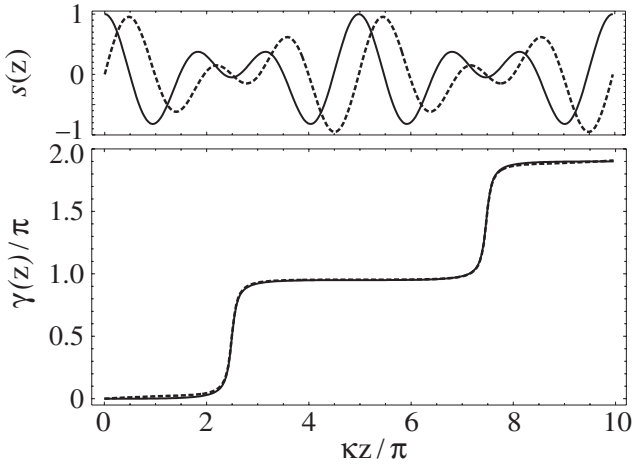

Figure 5. Geometric phase decomposition for polarization rotation with ellipticity parameter $Z = 0.05$ and coefficient of anisotropy $\delta/\kappa = 0.2$. Top, real (solid curve) and imaginary (dashed curve) parts of the complex signal. Bottom, true (solid curve) and estimated (dashed curve) geometric phases. STFT parameters: window width $\sigma = 0.75\delta = 0.15\kappa$, oversampling $K/N = 64$ and minimum spectral level 10^{-2}.

where

$$\phi_{\mathrm{d}}(\beta) = \delta \sin^2 \beta. \tag{62}$$

This case is rather different from the previous examples in that it considers the geometric phase dependence on the chosen parameter—rotation angle β of the birefringent plate, but not the temporal or spatial evolution. This results in a badly defined complex signal (58), which for some values of δ near 180° becomes a real sinusoidal signal. Such a signal has only linear phase dependence on the parameter β and there is no way to define the geometric phase. Therefore, instead of (58), the signal reconstructed only from the phase $\phi(\beta)$

$$s(\beta) = \mathrm{e}^{\mathrm{i}\phi(\beta)} \tag{63}$$

is chosen. Although its imaginary part also vanishes for the same values of δ, it is no longer a sinusoidal signal with trivial phase dependence. The real part now includes a part of the phase information of the original signal. Real and imaginary parts of the signal for several values of parameter δ are shown in figure 6. For some values of δ, the signal has steep edges, therefore it is sampled by a relatively large number—1024—of samples. True and estimated geometric phases are also shown in figure 6. The window bandwidth $\sigma = 2.5 \cdot 2\pi/T$ is chosen with respect to period $T = 360°$ of the rotation angle and is the same for all cases of δ. Different values of δ correspond to different contours in the parametric space—the Poincaré sphere. Geometric phase jumps $\pm\pi$ near $\delta = 180°$ coincide with the great circles on the Poincaré sphere. Signals in parts (*c*) and (*d*) of figure 6 differ by the sign of the imaginary part, which is small in absolute value, but inverts the sign of the total phase. Although there is no perfect agreement between theoretical and numerical results, the estimated geometric phase clearly exhibits its characteristic features—nonlinearity and phase jumps.

6. Conclusions

The proposed method for geometric phase estimation from the scalar vector product of the final and initial states employs the time–frequency distribution of the corresponding complex

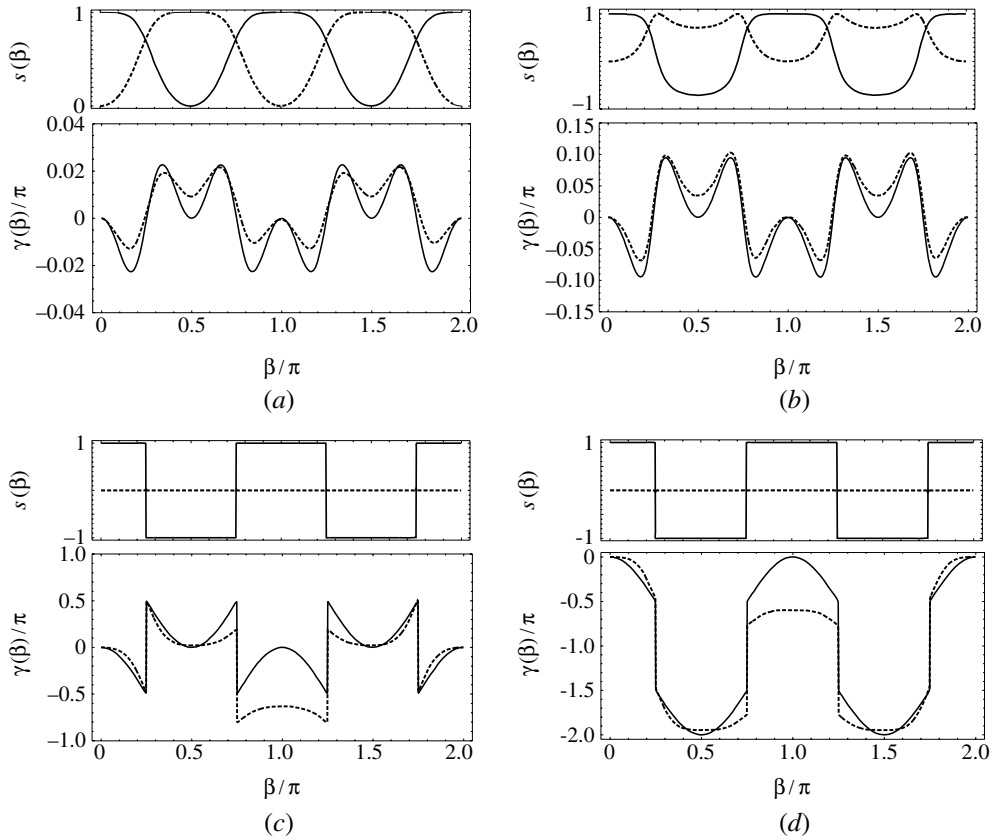

Figure 6. Geometric phase decomposition for polarization birefringence for various values of retardation: 89.99° (*a*), 135° (*b*), 179.99° (*c*) and 180.01° (*d*). Top of each plot, real (solid curve) and imaginary (dashed curve) parts of the complex signal. Bottom of each plot, true (solid curve) and estimated (dashed curve) geometric phases. STFT parameters: window width $\sigma = 2.5 \cdot 2\pi/T$, $T = 360°$, oversampling $K/N = 256$ and minimum spectral level 10^{-2}.

signal. The resulting geometric phase depends on the STFT window width. As shown in the above examples, by proper adjustment of the window width, a suitable agreement between true and estimated geometric phases can be achieved. This produces satisfactory results even for badly defined signals, reconstructed from the phase alone. The window width is not known in advance and has to be determined on the basis of theoretical results, but once determined for a given system it can be used for all cases of the system's evolution.

Another drawback of the method is that it is prone to sampling errors. Averaging over frequency with respect to the numerically obtained time–frequency distribution is significantly biased by the small values of the distribution. Therefore, for real-world signals, the spectrum must be bounded by a minimum level for which integration is performed.

Nevertheless, the method represents an alternative for theoretical decomposition of geometric phase and in this perspective may be used for experimental evaluation of the geometric phase. The results may be important especially because to date there is no purely experimental way to determine the geometric phase without detailed knowledge of the system's evolution model.

Acknowledgment

This research has been supported by the Lithuanian State Science and Studies Foundation.

References

[1] Berry M V 1984 *Proc. R. Soc.* A **392** 45
[2] Anandan J, Christian J and Wanelik K 1997 *Am. J. Phys.* **65** 180
[3] Bhandari R 1997 *Phys. Rep.* **281** 1
[4] Aleksiejunas R and Ivaska V 1997 *Phys. Lett.* A **235** 1
[5] Pancharatnam S 1956 *Proc. Ind. Acad. Sci.* A **44** 247
[6] Samuel J and Bhandari R 1988 *Phys. Rev. Lett.* **60** 2339
[7] Suter D, Mueller K T and Pines A 1988 *Phys. Rev. Lett.* **60** 1218
[8] Wagh A G *et al* 1997 *Phys. Rev. Lett.* **78** 755
[9] Aleksiejunas R and Ivaska V 2000 *J. Phys. A: Math. Gen.* **33** 2383
[10] Cohen L 1995 *Time–Frequency Analysis* (Englewood Cliffs, NJ: Prentice-Hall)
[11] Qian S and Chen D 1996 *Joint Time–Frequency Analysis: Methods and Applications* (Englewood Cliffs, NJ: Prentice-Hall)
[12] McLaughlin J 1997 Applications of operator theory to time–frequency analysis and classification *PhD Dissertation* University of Washington, Ann Arbor, MI
[13] Gabor D 1946 *J. Inst. Elec. Eng.* **93(III)** 429
[14] Bastiaans M J and Geilen M C W 1996 *Signal Process.* **49** 151
[15] Wagh A G, Rakhecha V C, Fischer P and Ioffe A 1998 *Phys. Rev. Lett.* **81** 1992
[16] Wagh A G and Rakhecha V C 1992 *Phys. Lett.* A **170** 71
[17] Wagh A G and Rakhecha V C 1993 *Phys. Rev.* A **48** R1729
[18] Wagh A G and Rakhecha V C 1995 *Phys. Lett.* A **197** 112
[19] Klyshko D N 1993 *Usp. Fiz. Nauk* **36** 1005
[20] Bhandari R 1991 *Phys. Lett.* A **157** 221
[21] Wagh A G and Rakhecha V C 1995 *Phys. Lett.* A **197** 107
[22] Badurek G, Rauch H and Tuppinger D 1986 *Phys. Rev.* A **34** 2600
[23] Wagh A G and Rakhecha V C 1996 *Prog. Part. Nucl. Phys.* **37** 485
[24] Simon R, Kimble H J and Sudarshan E C G 1988 *Phys. Rev. Lett.* **61** 19